Proceedings of Meetings on Acoustics

Volume 28 http://acousticalsociety.org/

22nd International Congress on Acoustics
Acoustics for the 21st Century

Buenos Aires, Argentina
05-09 September 2016

Signal Processing in Acoustics: Paper ICA2016-614

Cross-frequency coupling and phase synchronization in nonlinear acoustics

Damián Dellavale
Laboratorio de Bajas Temperaturas, Centro Atómico Bariloche, CONICET, Instituto Balseiro, R8402AGP, Río Negro, Argentina; dellavale@cab.cnea.gov.ar

Juan Manuel Rosselló
Laboratorio de Cavitación y Biotecnología, Centro Atómico Bariloche, CONICET, Instituto Balseiro, R8402AGP, Río Negro, Argentina; jrossello@cab.cnea.gov.ar

The Cross-Frequency Coupling (CFC) characterizes the correlation between the phase/amplitude of a low-frequency band with those of a high-frequency band within or across time series. The CFC phenomenon has been observed in a variety of systems: earth seismic waves, stock market fluctuations, pulsatile hormone secretions and in the scale-free activity of the human brain. In this work, experiments were conducted using a liquid-filled spherical chamber arranged in an experimental setup tailored for characterizing the acoustic field developed in typical nonlinear dynamics found in bubbly liquid media, like single/multi-bubble sonoluminescence (SL). The measured time series data were analyzed using signal processing algorithms specialized for quantifying CFC and phase synchronization phenomena. Our results suggest that in absence of bubbles, the excitatory-inhibitory interaction among the acoustic modes of the spherical resonator, coupled via 1:n internal resonances, produces the nonlinear harmonics observed in the system response. On the other hand, it was found that the interaction between the acoustic modes of the spherical resonator with the SL bubble(s) acoustic emission, generates nonlinear harmonics amplitude-modulated by the phase of the fundamental driving frequency in which the overall modulation strength and its variance across multiple time series data depend on the spatial stability of the SL-bubble(s).

Published by the Acoustical Society of America

© 2016 Acoustical Society of America [DOI: 10.1121/2.0000294]

Redistribution subject to ASA license or copyright; see http://acousticalsociety.org/content/terms. Download to IP: 217.235.189.126 On: Mon, 07 Nov 2016 20:34:30

1 Introduction

Sonoluminescence (SL) is a physical phenomenon characterized by the emission of light pulses from a gas bubble which is forced to have periodic in time and highly nonlinear cycles of expansion and compression through the action of a driving sound wave. Under this situation, the energy focused in the spherically converging inertial collapses is enough to produce a sudden rise in the pressure, density and gas temperature within the bubble. Consequently, a hot plasma core is produced from the gas and a very short ($100ps - 2ns$) pulse of light is emitted (from infrared to ultraviolet) [1, 2, 3, 4]. In this work Phase-Amplitude Coupling measure (PAC) [5, 6], Phase Locking Value (PLV) [7] and Time-Locked Plot (TLP) [5] are used to analyze Cross-Frequency Coupling (CFC) and phase synchronization in nonlinear ultrasound fields measured from a spherical acoustic resonator under both non-cavitation and single/multi-bubble SL conditions.

2 Apparatus and experimental method

The experiments were conducted using a spherical acoustic chamber made of quartz ($60mm$ in outer diameter and approximately $1mm$ in thickness) described and characterized in Refs. [1, 2, 3]. The working liquid used was a degassed sulfuric acid aqueous solution 85% w/w (SA85) with concentrations of dissolved gas (argon or xenon) in the range of $0.001 \lesssim c_\infty/c_0 \lesssim 0.017$ [1, 3]. The eigenfrequency of the acoustic chamber for the lowest order radially symmetric oscillation mode, with a pressure antinode near the geometrical center of the flask, was experimentally determined in $f_0 \approx 29.2kHz$. The driving system was composed of two equal piezoceramic transducers (PZT) attached to the outer wall of the resonator in diametrically opposed positions (see Figure 1). The two PZT drivers were excited with the same electrical signal ($V_d = V_0\, sin(2\,\pi\, f_d\, t)$). A disc shaped pill PZT was fixed to the resonator outer wall to be used as an acoustic signal sensor (MIC). In the experiments, the acoustic pressure field was set by controlling the frequency (f_d) and the amplitude (V_0) of the electrical driving signal. We developed a tailored multi-frequency electronics for concurrent signal synthesis and measurement based on Field Programmable Gate Array (FPGA) technology [3, 8]. This custom instrumentation was arranged in an experimental setup specialized for characterizing the nonlinear harmonics present in the acoustic field. Figure 1 shows the experimental setup used for measuring the resonator response subject to a single-frequency driving signal applied to the PZT pair. The FPGA board provide, through a $12bits$ D/A converter with a sample rate of $f_s \gtrsim 10f_0$, a low-distortion sinusoidal signal tuned to the resonance of the acoustic chamber first mode ($f_0 \approx 29.2kHz$). In order to prevent introducing high-frequency artifact spuriously induced by the digital electronics, the driving signal is conditioned in amplitude (Pre-amp. *LF Amp.* in Figure 1) and then bandpass (BP) filtered (quality factor $Q \approx 10$) by the low-noise preamplifier *Stanford Research Systems Model SR650*. After that, signal amplification is implemented using a power audio amplifier (*Radioshack* $100w$, $V_{out}|_{max} = 70V_{rms}$)

Redistribution subject to ASA license or copyright; see http://acousticalsociety.org/content/terms. Download to IP: 217.235.189.126 On: Mon, 07 Nov 2016 20:34:30

which feeds a RLC_{PZT} circuit ($Q \approx 15$), tuned via the inductance L in order to maximize the voltage signal ($V_d|_{max} \approx 1000V_{rms}$) applied to the PZT drivers. It is worth noting that, a further BP filtering of the driving signal V_d occurs due to the narrow full-width half-power bandwidth $Bw_0 = f_0/Q \approx 117Hz$ of the acoustic resonator first mode (measured $Q \approx 250$) [2, 3]. The response of the acoustic resonator was constituted by the the MIC electrical signal, which is proportional to the acceleration of the resonator wall. The MIC was coupled to the high input impedance ($100M\Omega//25pF$) preamplifier and configurable BP filter *Stanford Research Systems Model SR560*. The *SR560* was configured as an anti-aliasing filter with a pass-band of $10kHz - 1MHz$. Then, the MIC signal was acquired by a *GW-Instek Model 2204* oscilloscope at a sampling rate of $2.5Msps$ and a memory depth of $25k$ samples [1]. In all the reported experiments, the bubbles were produced by acoustic cavitation near the center of the spherical resonator, were the main pressure antinode is located.

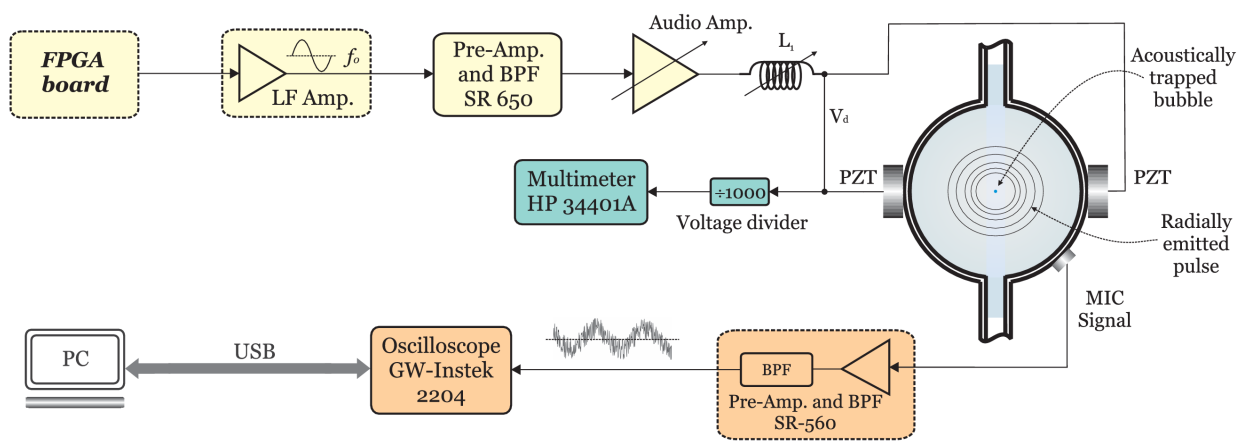

Figure 1: Experimental setup specialized for measuring the resonator response subject to a single-frequency driving signal applied to the PZT pair. The response of the acoustic resonator was constituted by the electrical signal obtained from the MIC, which is proportional to the acceleration of the spherical shell.

3 Results and discussion

In the following sections we analyze the nonlinear harmonics present in the acoustic field developed within the spherical resonator under four scenarios: 1. Absence of bubbles within the liquid-filled spherical shell (Label: *No-bubble*, $V_d \approx 200V_{rms}$), 2. Spatially stable single sonoluminescent bubble (Label: *Non-moving SBSL*, $V_d \approx 191V_{rms}$), 3. Single sonoluminescent bubble describing pseudo-

Redistribution subject to ASA license or copyright; see http://acousticalsociety.org/content/terms. Download to IP: 217.235.189.126 On: Mon, 07 Nov 2016 20:34:30

orbits (Label: *Moving SBSL*, $V_d \approx 204V_{rms}$) and 4. Multiple spatially unstable sonoluminescent bubbles (Label: *Moving MBSL*, $V_d \approx 260V_{rms}$).

3.1 Non-linear harmonics in the acoustic spectra

In this section we discuss the power spectra computed from the MIC signal collected with the experimental setup described in Section 2 (Figure 1). Figure 2 shows the Power Spectral Densities (PSD) corresponding to the four nonlinear acoustic scenarios described in section 3. All the PSD estimates shown in Figure 2 were computed from the MIC signal using the modified periodogram method. Windowing in time domain was implemented using a Gaussian function in order to be able to compute the quadratic interpolation technique to obtain the spectral peaks coordinates (amplitude and frequency) [3]. Thresholding of the power spectrum at 3 times the median value of its amplitude was used for peaks detection. We found that the frequencies of the detected spectral peaks match those of the harmonics Nf_0 of the fundamental component f_0 with a difference less than 0.1% [3]. In all the four cases shown in Figure 2, a single-frequency driving tuned to the resonance of the acoustic chamber first mode ($f_d = f_0 \approx 29.2kHz$) was used to drive the spherical shell. In the *No-bubble* case of Figure 2, spectral harmonic peaks located at Nf_0 with amplitudes greater than $\approx -40dB$ relative to the fundamental component (f_0) are observed for $N \lesssim 12$. Taking into account that the full-width half-power ($-3dB$) bandwidth of the liquid-filled shell for the first radially-symmetric acoustic mode is $Bw_0 = f_0/Q = 29.2kHz/250 \approx 117Hz$, it was found that by detuning the driving signal ($f_d \approx f_0 \pm 10Bw_0$) and keeping the driving amplitude V_0 unchanged, those harmonic peaks present in the *No-bubble* case (Figure 2) were attenuated in more than 2 orders of magnitude for $N = 2$ and attenuations greater than 4 orders of magnitude were observed for $N \geq 3$ [1] (not shown). The latter suggest that the amplitudes of harmonic peaks obtained in the *No-bubble* condition, are not completely explained by only considering a nonlinear behavior of the acoustic resonator. Instead, it appears that to account for the presence of the harmonic peaks, acoustic energy coupling from the first mode to others high-frequency modes (not necessarily radially symmetric), has to be considered besides the nonlinear behavior of the resonator. This hypothesis is consistent with the observed amplitude of the harmonic peaks in both resonance ($f_d = f_0$) and off-resonance ($f_d \approx f_0 \pm 10Bw_0$) driving conditions discussed above. It is important to note that, the coupling between the first mode with other acoustic modes is favored by the quadratic growth of the number of spherical normal modes with the frequency [3] and by the degeneracy of the non-radially symmetric modes [4]. Figure 3 shows that, in the case of *No-bubble* condition, as the driving amplitude is increased ($V_d \gtrsim 100V_{rms}$), acoustic energy is transferred from the fundamental spectral component (f_0) to its harmonics (Nf_0). More importantly, the decrease in the fundamental component amplitude match very well the increase of the summed amplitudes of nonlinear harmonics in the range $N = 2, 3, 4, 5$. This experimental result support the hypothesis that the observed spectral harmonics in the case of *No-bubble* condition are produced by $1 : n$ internal resonances with $n = 2, 3, 4, 5$. Besides, this inter-mode coupling can

Redistribution subject to ASA license or copyright; see http://acousticalsociety.org/content/terms. Download to IP: 217.235.189.126 On: Mon, 07 Nov 2016 20:34:30

be understood in terms of interacting systems in which an excitatory system receiving oscillatory driving (f_0) represents the acoustic resonator first mode and, inhibitory systems constituted by other modes, drain acoustic energy from the first mode reducing its amplitude [9]. The results discussed above provide quite strong experimental evidence suggesting that in absence of bubbles within the acoustic chamber the interaction among the acoustic modes of the spherical resonator, coupled via $1:n$ internal resonances, produces the nonlinear spectral harmonics (Nf_0) present in the system response. Moreover, the upper graph of Figure 4 shows that the observed nonlinear harmonics Nf_0 for $N < 15$ in the case of liquid-filled acoustic chamber without bubbles, are produced by the excitation of acoustic modes associated to the liquid-filled resonator, and are not related to the elastic modes of the spherical shell (air-filled resonator). On the other hand, the SBSL and MBSL cases presented in Figures 2 and 4 show that, the periodic shock-wave emission from the sonoluminescent bubble(s) acoustically trapped within the resonator produce high-frequency harmonics Nf_0 for $N > 15$, which exhibits significantly higher amplitudes when compared with those observed in the *No-bubble* condition [1, 2, 3, 4].

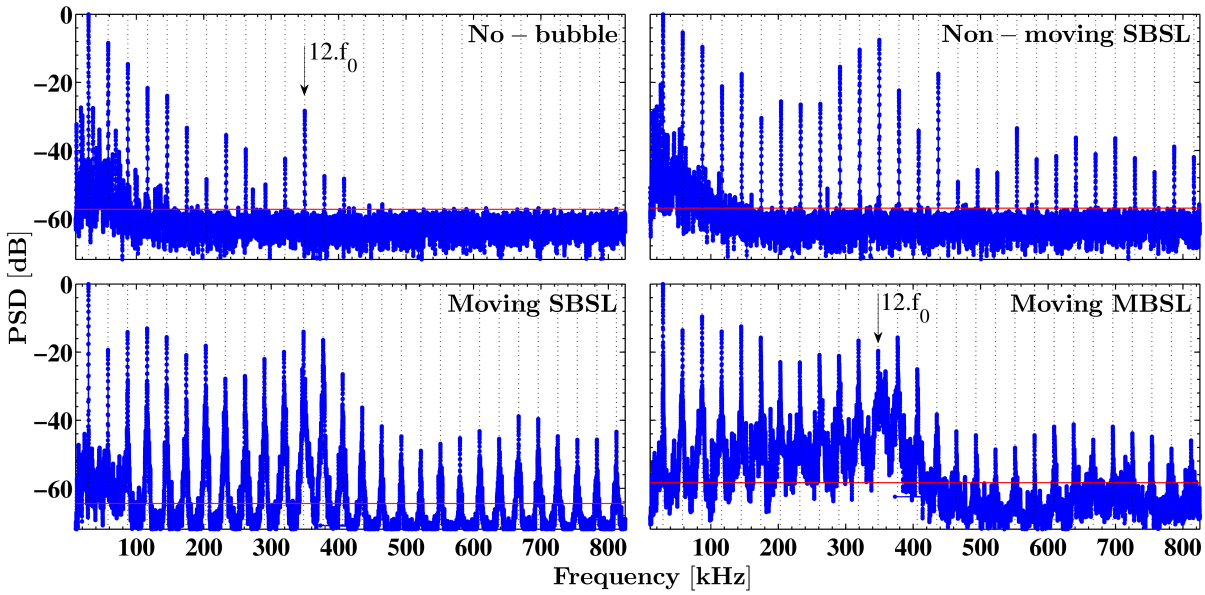

Figure 2: Acoustic spectra (PSD) computed from MIC signals corresponding to the four nonlinear acoustic scenarios. Each graph shows the average between 4 to 10 PSD estimates computed using the modified periodogram method with a Gaussian window in time domain. The horizontal solid lines (red) are the thresholds at 3 times the median value of the PSD amplitude, which were used for the peaks detection. The vertical dashed lines indicates the exact position of the harmonic frequencies (Nf_0).

Redistribution subject to ASA license or copyright; see http://acousticalsociety.org/content/terms. Download to IP: 217.235.189.126 On: Mon, 07 Nov 2016 20:34:30

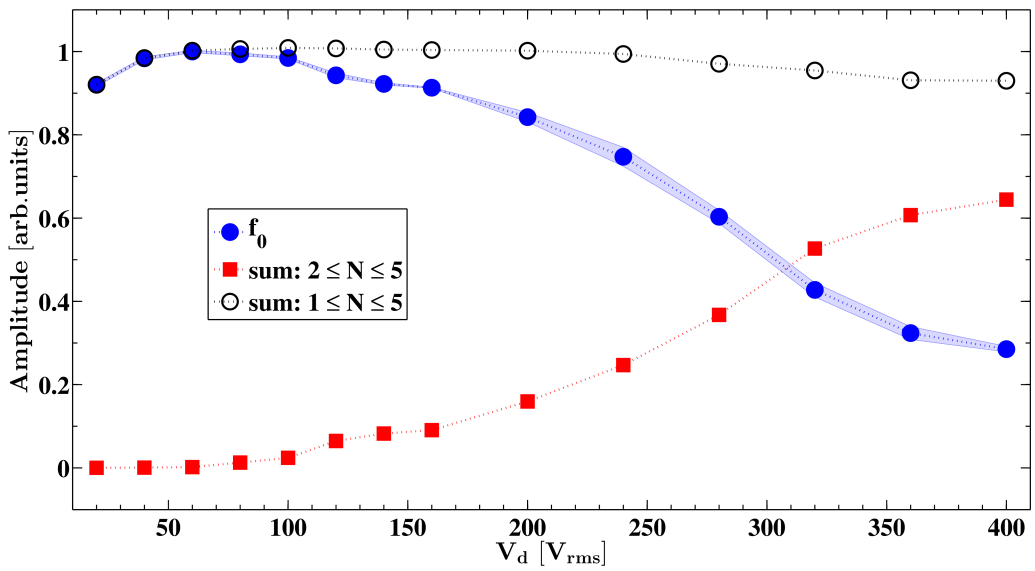

Figure 3: Amplitude of the spectral peaks observed in the PSD as a function of the driving voltage (V_d) in the case of *No-bubble* condition. The decrease in the amplitude of the fundamental component (f_0, filled circles) mirrors the increase of the summed amplitudes of nonlinear harmonics in the range $2 \leq N \leq 5$ (filled squares). The shaded error bars shown for the fundamental component are the standard deviation of 4 PSD value at each point. The empty circles are the summed PSD amplitudes corresponding to the fundamental component f_0 besides the harmonics Nf_0 for $2 \leq N \leq 5$. The almost constant amplitude of this sum (empty circles) evince the acoustic energy coupling from the fundamental component to its harmonics.

3.2 Phase-amplitude cross-frequency coupling

In this section we analyze the response of the acoustic resonator using an algorithm for estimating the phase-amplitude cross-frequency coupling. Our algorithm computes a modulation index (MI) for estimating PAC based on a normalized entropy measure and have been implemented following the Ref. [5], including two major modifications related to the filtering stage. First, we use 4th order Butterworth BP filters constructed by the cascade connection of a 2nd order high-pass filter followed by a 2nd order low-pass filter [10]. Then, the signal is filtered twice, forward and backward, in order to ensure that phase delays introduced by the filter are nullified. Second, adaptive BP filtering for the frequencies for amplitude (ordinate axis of the comodulogram) was implemented following Ref. [11]. Thus, each BP filter corresponding to the ordinate axis of the comodulogram was centered at the harmonic frequency of interest Nf_0 (for $1 \leq N \leq 42$) and the cutoff frequencies

Redistribution subject to ASA license or copyright; see http://acousticalsociety.org/content/terms. Download to IP: 217.235.189.126 On: Mon, 07 Nov 2016 20:34:30

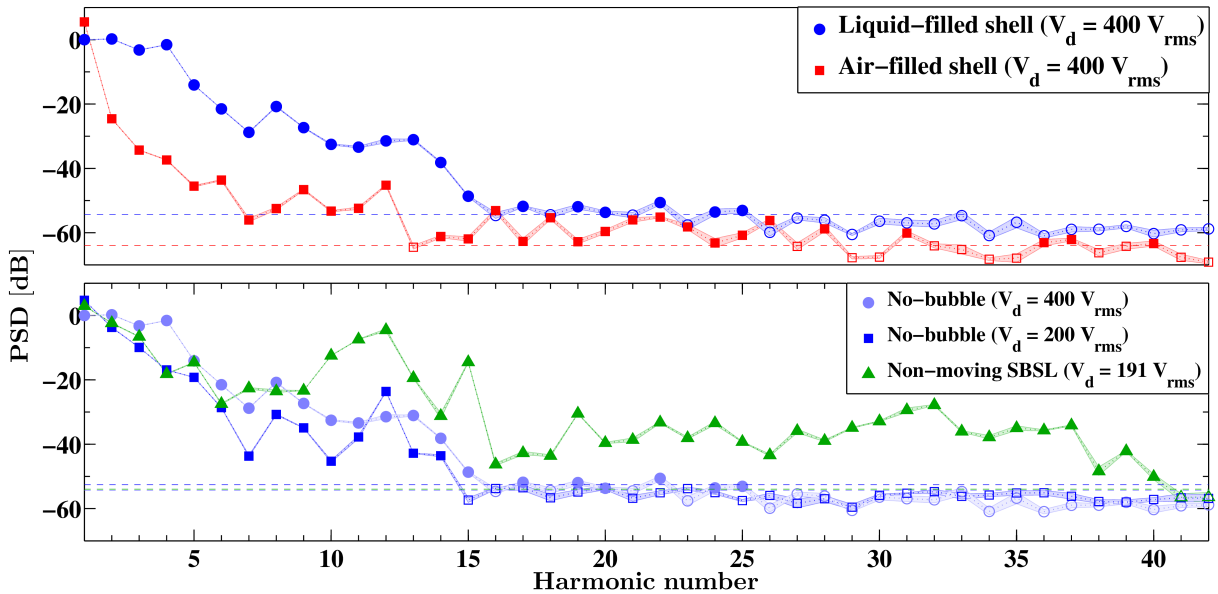

Figure 4: Amplitude of the spectral peaks as a function of the harmonic number (N). The dashed lines are the thresholds at 3 times the median value of the PSD amplitude, which were used for the peaks detection. Only the PSD amplitudes above those threshold were recorded as spectral peaks and are indicated with filled markers. On the other hand, empty markers correspond to PSD amplitudes below the threshold level, i.e, no peak detected at that harmonic frequency. The shaded error bars correspond to the standard deviation of 4 PSD value at each point. (*Upper*) The circles are the detected peaks in the case of liquid-filled acoustic chamber in absence of bubbles. Square markers correspond to the peaks for the air-filled acoustic chamber. (*Lower*) Portrait of the spectral peaks for the *Non-moving SBSL* condition compares with the *No-bubble* at two driving voltages. Circles in the upper and lower graphs correspond to the same condition (Liquid-filled resonator in absence of bubbles drived at $V_d \approx 400 V_{rms}$).

($-3dB$) were automatically configured at $Nf_0 \pm f_0$. It is important to point out that, due to the finite slope of the BP filter transition edges, there are considerable overlap between adjacent frequency bands. That is, the output BP filtered signal contains residual off-band frequencies. As a consequence, adjacent frequency bands used to compute the PAC, PLV and TLP measures should not be considered independent. For further details about the algorithms for estimating PAC the reader is referred to Refs. [6, 10]. Figure 5 displays the comodulograms, as contour plots of the MI values, computed from the MIC signal corresponding to the four acoustic scenarios studied in this work. The modulation index (MI) quantifies the strength of the correlation between the phase of the fundamental frequency f_0 (abscissa of the comodulogram) with the amplitude envelope of the

Redistribution subject to ASA license or copyright; see http://acousticalsociety.org/content/terms. Download to IP: 217.235.189.126 On: Mon, 07 Nov 2016 20:34:30

BP filtered signal centered at Nf_0 (ordinate of the comodulogram). It should be noted that the MI measure is sensitive to the amplitude of the side-bands ($(N \pm 1)f_0$) relative to the amplitude of the modulated spectral component (Nf_0). That is, the bigger the amplitude of the side-bands relative to that of the modulated spectral component Nf_0, the deeper the amplitude modulation of Nf_0 resulting in a higher MI value. This behavior produces the local maxima of MI values shown in the comodulograms of Figure 5. In the *No-bubble* case of Figure 5, significant MI values are observed up to $N \approx 12$. This result is consistent with the power spectra shown in Figure 2 for the *No-bubble* condition, in which no harmonic peaks occurs for $N \gtrsim 12$. On the other hand, for the *Non-moving SBSL*, *Moving SBSL* and *Moving MBSL* cases shown in Figure 5, non-vanishing MI values extend up to $N \approx 30$ due to the presence of high-frequency harmonics produced by the acoustic emission of the SL bubble(s). Since the MI measure shown in Figure 5 is highly independent on the absolute level of the amplitude-modulated frequency (i.e, the amplitude of the harmonic peaks) [6], PAC is detected for these high-frequency harmonics despite the decrease in their amplitude that takes place as the frequency increases (see Figure 2). The acoustic field developed in the *Moving SBSL* and *Moving MBSL* cases results non-stationary due to the pseudo-orbits described by the SL bubble(s). This non-stationary nature of the acoustic field produces degenerate non-harmonic spectral components forming a bump centered around each harmonic peak at Nf_0, which can be identified in the power spectra shown in Figure 2. As a consequence, for the *Moving SBSL* and *Moving MBSL* cases the overall PAC strength is diminished (Figure 5) and the variance of the MI values across time series data is augmented (not shown), regarding of those observed for the *Non-moving SBSL* case.

3.3 Phase locking value

The PLV method was developed to look at phase-locking between signals (i.e, phase-phase coupling) and has been thoroughly described in the literature [7, 6]. Figure 6 shows the PLV between the phase of the fundamental frequency f_0 and the phase of the BP filtered signal centered at Nf_0, computed from the MIC signal and using the same BP filtering configuration of that used to compute the comodulograms presented in Figure 5 (see Section 3.2), but in this case the BP filter cutoff frequencies ($-3dB$) were settled at $Nf_0 \pm f_0/2$. Taking into account that the $|PLV|$ lies in the range $[0, 1]$, the *No-bubble* and *Non-moving SBSL* cases shown in Figure 6 exhibit relatively high PLVs for the low-order harmonics, which then gradually decrease with the increase of the harmonic order up to about $10f_0$, where a local increase in the PLVs occurs around $12f_0$. This behavior is related to the high amplitude of the harmonic peaks about $12f_0$ observed in the power spectra (see Figures 2 and 4), which in turn is the result of two possible underlying mechanisms: a) A piezoelectric resonance of the ultrasonic transducer (MIC) [3], and b) A strong coupling between the acoustic emission of the SL bubble(s) and oscillation modes of the resonator with eigenfrequencies close to $12f_0$ [2, 3]. Another important result from Figure 6 is that the PLVs for the *Moving SBSL* and *Moving MBSL* cases show a significantly higher variance when compared

Redistribution subject to ASA license or copyright; see http://acousticalsociety.org/content/terms. Download to IP: 217.235.189.126 On: Mon, 07 Nov 2016 20:34:30

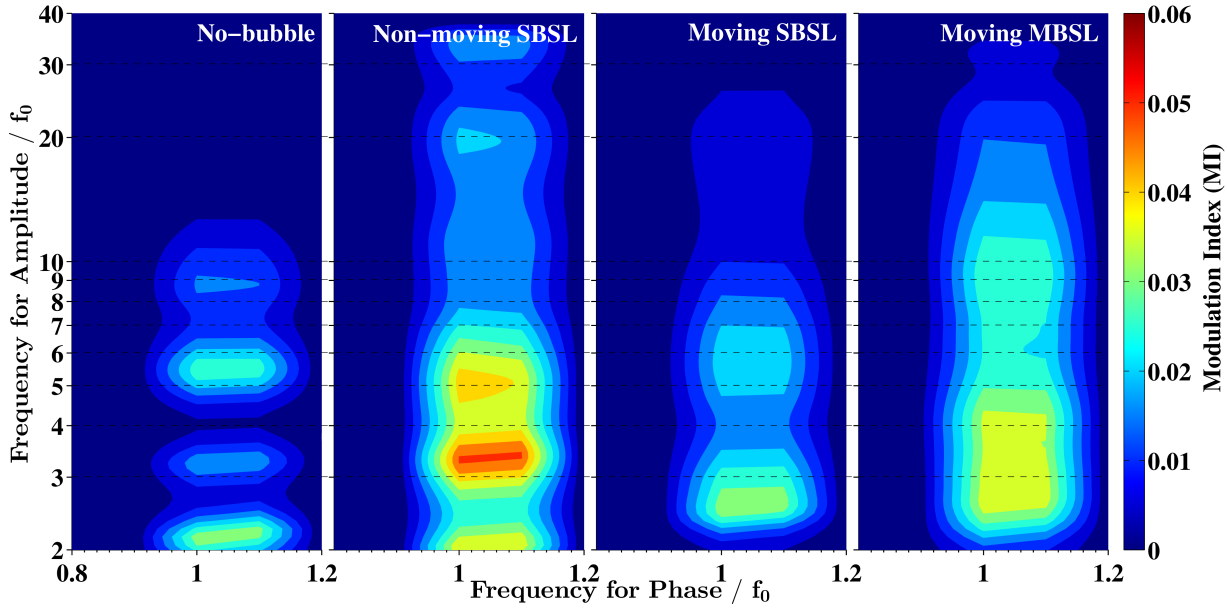

Figure 5: Comodulograms computed from MIC signals corresponding to the four nonlinear acoustic scenarios. Each contour plot shows the average between 4 to 10 comodulograms based on a normalized entropy MI measure.

to those for the *Non-moving SBSL* case. This behavior is due to the presence of non-harmonic side-bands around the harmonic peaks at Nf_0, brought about by the non-stationary nature of the acoustic field associated to the pseudo-orbits described by the SL bubble(s) in the *Moving SBSL* and *Moving MBSL* cases.

3.4 Time-locked plot

In this section we analyze the TLPs in relation to the results shown in Figures 5 and 6 corresponding to PAC and PLV measures, respectively. The computation of the TLPs have been implemented following the Ref. [5] using the same BP filtering configuration of that used to compute the PLVs presented in Figure 6 (see Section 3.3). Figure 7 shows that the fundamental component f_0 (dashed line) almost vanish from the mean signal trace (solid line) for the *No-bubble* case. This result indicates that the BP filtered signal centered at $12f_0$ is weakly amplitude-modulated by the fundamental frequency (f_0), in agreement with the corresponding comodulogram shown in Figure 5 and also with the small amplitude of the side-bands ($11f_0$ and $13f_0$) relative to the amplitude of the modulated component ($12f_0$) observed in the power spectrum shown in Figure 2 (*No-bubble* case). Moreover, the relatively high amplitude of the harmonic component $12f_0$ for the *No-bubble*

Redistribution subject to ASA license or copyright; see http://acousticalsociety.org/content/terms. Download to IP: 217.235.189.126 On: Mon, 07 Nov 2016 20:34:30

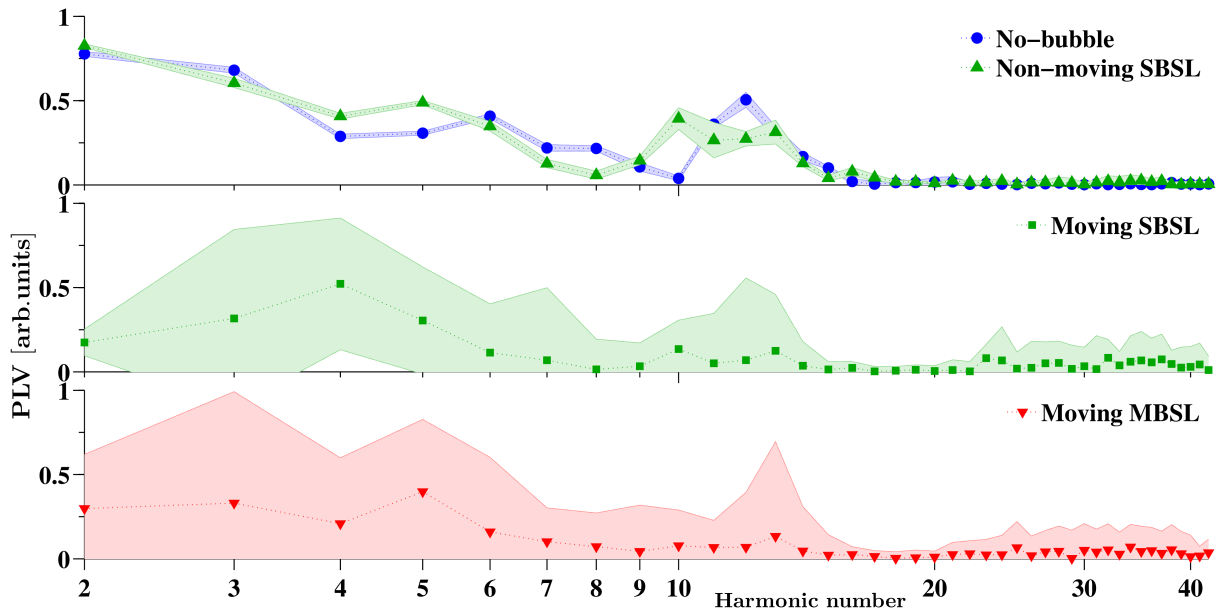

Figure 6: Phase-Locking Values computed from MIC signals corresponding to the four nonlinear acoustic scenarios. The filled markers results from the average between 4 to 10 phase-locking value at each point and the shaded error bars are the corresponding standard deviation.

case shown in Figure 7, indicates a strong phase-locking between the fundamental frequency (f_0) and the BP filtered signal centered at $12f_0$, resulting in a high PLV as shown in Figure 6 for the *No-bubble* case. In the *Non-moving SBSL* case shown in Figure 7, relatively high amplitudes were obtained for the harmonic $12f_0$ and the fundamental f_0 frequencies indicating that a strong phase-locking and phase-amplitude coupling, respectively, occurs between these two BP filtered signals centered at f_0 and $12f_0$ (see Figures 6 and 5). Due to the high variance of the MI values obtained for the *Moving SBSL* and *Moving MBSL* cases, the amplitude of the fundamental component f_0 (dashed line) shown in the TLP for those cases is diminished regarding of that obtained for the *Non-moving SBSL* case (Figure 7).

4 Conclusions

In this work for first time PAC, PLV and TLP algorithms are used to analyze cross-frequency coupling and phase synchronization in ultrasound fields developed within acoustic resonators driven to nonlinear oscillation regimes under both non-cavitation and single/multi-bubble SL conditions. Our results provide experimental evidence suggesting that in absence of bubbles within the acoustic chamber, the interaction among the acoustic modes of the spherical resonator, coupled via

Redistribution subject to ASA license or copyright; see http://acousticalsociety.org/content/terms. Download to IP: 217.235.189.126 On: Mon, 07 Nov 2016 20:34:30

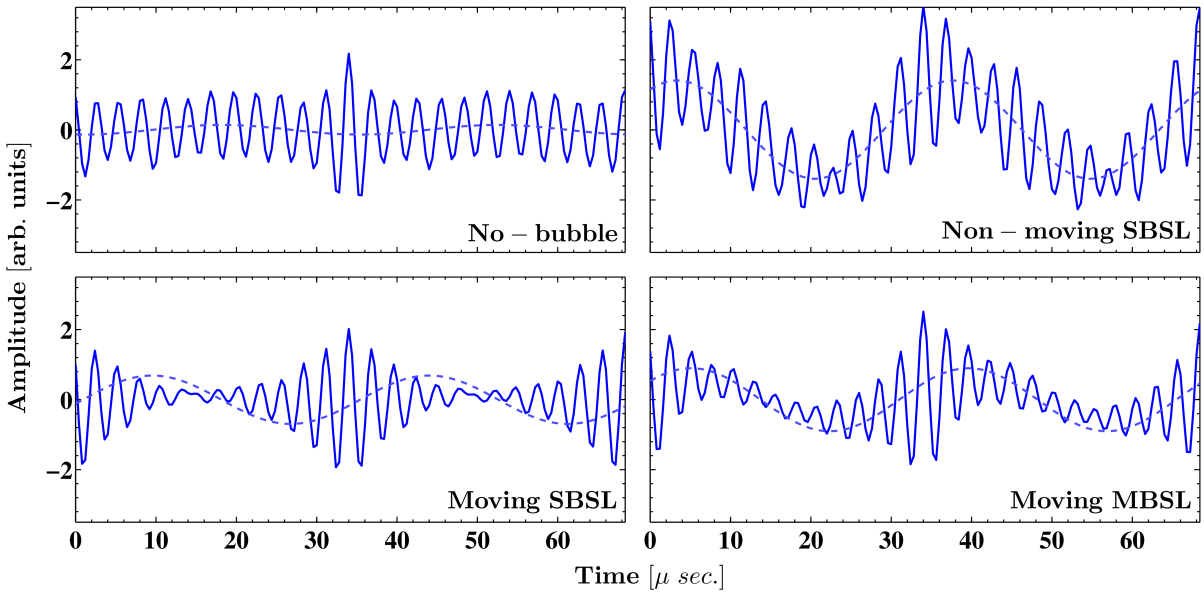

Figure 7: Time-locked plots computed from MIC signals corresponding to the four nonlinear acoustic scenarios. Each final trace (solid line) was obtained by averaging time windows of the raw MIC signal of two fundamental period ($2/f_0$) in width, centered at the maximum amplitude of the BP filtered signal at $12f_0$ in the same time window. The averaged signal trace (solid line) was then Fourier transformed at the fundamental frequency f_0 by fitting a sine function (dashed line).

$1:n$ internal resonances, produces the observed nonlinear spectral harmonics (Nf_0) in the system response. It was found that, the non-stationary nature of the acoustic field associated to the pseudo-orbits described by the SL bubble(s) in the *Moving SBSL* and *Moving MBSL* cases, produces degenerate non-harmonic side-bands forming a bump centered around each harmonic peak at Nf_0. As a consequence, the overall PAC strength for the *Moving SBSL* and *Moving MBSL* cases is diminished regarding of that observed for the *Non-moving SBSL* case. For the same reason, the PLV and MI measures for the *Moving SBSL* and *Moving MBSL* cases show a significantly higher variance across multiple time series data, when compared to those observed for the *Non-moving SBSL* case.

Redistribution subject to ASA license or copyright; see http://acousticalsociety.org/content/terms. Download to IP: 217.235.189.126 On: Mon, 07 Nov 2016 20:34:30

References

[1] J. M. Rosselló, Ph.D. Thesis, Frontera de estabilidad en sonoluminiscencia y concentración de energía en cavitación transitoria forzada, Instituto Balseiro - Argentina (2015).

[2] D. Dellavale, et al. Analytical study of the acoustic field in a spherical resonator for single bubble sonoluminescence, J. Acoust. Soc. Am. 127 (1), 2010, 186-197.

[3] D. Dellavale, Ph.D. Thesis, Algoritmos para el procesamiento concurrente de señales y su aplicación en sonoluminiscencia, Instituto Balseiro - Argentina (2011).

[4] F. B. Seeley, Effects of higher-order modes and harmonics in single-bubble sonoluminescence, J. Acoust. Soc. Am. 105 (4), (1999) 2236-2242.

[5] A. B. L. Tort, et al. Dynamic cross-frequency couplings of local field potential oscillations in rat striatum and hippocampus during performance of a T-maze task. Proc Natl Acad Sci USA, 105(51), (2008) 20517-20522.

[6] A. B. L. Tort, et al. Measuring phase-amplitude coupling between neuronal oscillations of different frequencies. J. of Neurophysiol., 104(2), (2010) 1195-1210.

[7] J.P. Lachaux, et al. Measuring phase synchrony in brain signals, Hum Brain Mapp., 8(4), (1999) 194-208.

[8] D. Dellavale, et al. FPGA based Multi-Harmonic Control System for Single Bubble Sonoluminescence, 4th Southern Conference on Programmable Logic (IEEE, 2008), p.269.

[9] Angela C. E. Onslow et al. A Canonical Circuit for Generating Phase-Amplitude Coupling, PLoS ONE 9(8): e102591 (2014).

[10] B. J. He, et al. The temporal structures and functional significance of scale-free brain activity. Neuron, 66(3), (2010) 353-369.

[11] J. I. Berman, et al. Variable Bandwidth Filtering for Improved Sensitivity of Cross-Frequency Coupling Metrics. Brain Connectivity, 2(3), (2012) 155-163.

Redistribution subject to ASA license or copyright; see http://acousticalsociety.org/content/terms. Download to IP: 217.235.189.126 On: Mon, 07 Nov 2016 20:34:30